Ceramide-induced formation of ROS and ATP depletion trigger necrosis in lymphoid cells

Joan Villena [a,b,1], Mauricio Henriquez [a,1], Vicente Torres [a], Francisco Moraga [c], Jessica Díaz-Elizondo [c], Cristian Arredondo [a], Mario Chiong [c], Claudio Olea-Azar [c], Andres Stutzin [a], Sergio Lavandero [a,c], Andrew F.G. Quest [a,*]

[a] *Centro FONDAP Estudios Moleculares de la Celula (CEMC), Instituto Ciencias Biomedicas, Facultad de Medicina, Universidad de Chile, Santiago, Chile*
[b] *Departamento de Nutricion y Alimentos, Facultad de Farmacia, Universidad de Valparaíso, Valparaíso, Chile*
[c] *Centro FONDAP Estudios Moleculares de la Celula (CEMC), Facultad Ciencias Quimicas y Farmaceuticas, Universidad de Chile, Santiago, Chile*

Abstract

In lymphocytes, Fas activation leads to both apoptosis and necrosis, whereby the latter form of cell death is linked to delayed production of endogenous ceramide and is mimicked by exogenous administration of long- and short-chain ceramides. Here molecular events associated with noncanonical necrotic cell death downstream of ceramide were investigated in A20 B lymphoma and Jurkat T cells. Cell-permeable, C6-ceramide (C6), but not dihydro-C6-ceramide (DH-C6), induced necrosis in a time- and dose-dependent fashion. Rapid formation of reactive oxygen species (ROS) within 30 min of C6 addition detected by a dihydrorhodamine fluorescence assay, as well as by electron spin resonance, was accompanied by loss of mitochondrial membrane potential. The presence of *N*-acetylcysteine or ROS scavengers like Tiron, but not Trolox, attenuated ceramide-induced necrosis. Alternatively, adenovirus-mediated expression of catalase in A20 cells also attenuated cell necrosis but not apoptosis. Necrotic cell death observed following C6 exposure was associated with a pronounced decrease in ATP levels and Tiron significantly delayed ATP depletion in both A20 and Jurkat cells. Thus, apoptotic and necrotic death induced by ceramide in lymphocytes occurs via distinct mechanisms. Furthermore, ceramide-induced necrotic cell death is linked here to loss of mitochondrial membrane potential, production of ROS, and intracellular ATP depletion.

Keywords: Ceramide; Reactive oxygen species; Necrosis

Introduction

The lipid second messenger ceramide is implicated in the regulation of cell growth, proliferation, senescence, and death [1]. Such pleiotropism is indicative of many potential downstream effectors that may be linked to cell-specific differences, the generation of ceramide at a variety of subcellular sites, and the formation of additional signaling molecules via ceramide turnover, to mention just a few possibilities.

A large body of evidence associates ceramide generation with induction of cell death and ceramide has been referred to as a "coordinator" of cell stress. Consistent with this view, ceramide formation has been observed in cells in response to cytokines (FasL, Fas ligand; TNFα, tumor necrosis factor; IL-1β

Abbreviations: 3-ABA, 3-aminobenzamide; ATP, adenosine triphosphate; C6, C6-ceramide; Cat, catalase; DH-C6, dihydro-C6-ceramide; DHR123, dihydrorhodamine 123; DMSO, dimethyl sulfoxide; DMPO, 5,5-dimethyl-1-pyrroline-*N*-oxide; DNTB, 5,5′-dithiobis-2-nitrobenzoic acid; EDTA, ethylenedinitrilotetraacetic acid; ESR, electron spin resonance; FasL, Fas ligand; GSH, glutathione; IL-1β, interleukin-1β; LDH, lactate dehydrogenase; MOI, multiplicity of infection; MPT, mitochondrial permeability transition; NAC, *N*-acetylcysteine; NGF, nerve growth factor; PARP, poly(ADP-ribosyl) polymerase; PCD, programmed cell death; PI, propidium iodide PMSF, phenylmethylsulfonyl fluoride; ROS, reactive oxygen species; Tir, Tiron; TNFα, tumor necrosis factor α; Tr, Trolox.

* Corresponding author. Instituto Ciencias Biomedicas, Facultad de Medicina, Universidad de Chile, Independencia 1027, Santiago, Chile. Fax: +56 2 7382015.
E-mail address: aquest@med.uchile.cl (A.F.G. Quest).

[1] These authors contributed equally to this work.

interleukin-1β; and NGF, nerve growth factor), environmental stress (heat, UV, irradiation, hypoxia/reperfusion), and chemotherapeutic agents (Ara-C, doxorubicin, etoposide, etc) [1]. Ceramide is generated as an intermediate in the synthesis of sphingomyelin and complex glycosphingolipids. Hence, ceramide accumulation in response to stress generally results from either enhanced degradation of sphingolipids via neutral or acidic sphingomyelinases or via the "de novo" synthesis pathway. However, ceramide also accumulates as a consequence of changes in clearance via sphingomyelin synthases or ceramidases [1].

Ceramide modulates the activity of a large number of signaling proteins including phosphatases (PP1, protein phosphatase 1; PP2, protein phosphatase 2), kinases (Akt/PKB, protein kinase B; KSR, kinase suppressor of Ras; PKCs, protein kinase Cs), and phospholipases (PLA2, phospholipase A2), as well as proteases (cathepsin D) [1,2] and may promote different forms of cell death. In addition, ceramide directly modulates mitochondria function, for instance, by inhibiting the mitochondrial respiratory complex III [3–5], where the ubiquinone pool is an important site for production of ROS.

ROS produced by organelles, such as mitochondria [6], or at the plasma membrane due to NADPH oxidases [7] are established pathophysiological regulators of gene transcription, proliferation, and apoptosis [6]. Also, ROS production observed in response to a variety of chemical stimuli triggers necrosis via stimulation of lipid peroxidation and overall perturbation of the cellular redox status [8,9].

Cells demonstrate a high degree of flexibility in cell death responses, as is reflected by a variety of mechanisms, including apoptosis or type I programmed cell death (PCD), necrosis-like PCD, autophagy (or type II PCD), and accidental necrosis. The precise nature of molecular events associated with various noncanonical PCD pathways is not well understood. Apoptosis is the result of a highly orchestrated sequence of biochemical events that leads to orderly cell disassembly. Necrosis, in contrast, is thought to be the passive consequence of massive cell damage and hence accidental, uncontrolled, and harmful by nature. However, recent data suggest that this simplistic view may need to be revised [10,11].

Our previous results show that Fas ligand induces both an apoptosis and an alternative form of death, referred to as necrosis, in the same population of A20 B-lymphoma and Jurkat T cells [12]. Moreover, delayed elevation of endogenous ceramide is proposed to promote necrosis in those Fas-stimulated cells where caspase-8 activation is insufficient to trigger apoptosis. Interestingly, cell-permeable ceramides induce cell death in A20, Jurkat, and Raji cells essentially in the absence of caspase activation, DNA fragmentation, thus in a fashion reminiscent of FasL-induced necrosis. Indeed, morphologically, FasL-induced necrosis and cell death induced by cell-permeable ceramides are indistinguishable [12].

The molecular mechanisms downstream of ceramide that result in alternative forms of cell death, like necrosis, remain poorly characterized. Here, we sought to elucidate the role of ROS in determining ceramide-induced cell fate. Our data suggest that ROS produced due to ceramide-mediated mitochondrial damage drives cells toward necrotic death via ATP depletion.

Materials

Cell media and antibiotics were from Invitrogen (Carlsbad, CA). Fetal calf serum was from Hyclone (Logan, UT). C6, DH-C6, and caspase inhibitors (Ac-DEVD-cho, Ac- YVAD-cho, zVAD-fmk) were from Alexis Biochemicals (Lausanne, Switzerland). Soluble recombinant human FasL was from Apotech (Lausanne, Switzerland). 5,5-Dimethyl-1-pyrroline-*N*-oxide (DMPO), ethylenedinitrilotetraacetic acid (EDTA), glutathione (GSH), reduced form of nicotinamide adenine dinucleotide phosphate (NADPH), phenylmethylsulfonyl fluoride (PMSF), Trolox, Tiron, *N*-acetylcysteine (NAC), rhodamine 123, dyhydrorhodamine 123, and 3-aminobenzamide (3-ABA) were from Sigma (St. Louis, MO). The CitoTox 96 kit and Cell-Titer Glo kit were from Promega (Madison, WI). The BCA reagent was from Pierce (Rockford, IL).

Methods

Cell culture

A20 B lymphoma cells were cultured in DMEM (4.5 g glucose/liter) supplemented with 10% fetal calf serum, antibiotics (10,000 U/ml penicillin, 10 μg/ml streptomycin), and 50 μM ethanol-2-thiol at 37°C and 5% CO_2 as previously described [12]. Jurkat T cells were cultured in RPMI (1.8 g glucose/liter) supplemented with 10% fetal calf serum and antibiotics (10,000 U/ml penicillin, 10 μg/ml streptomycin).

Viability assays

Cell viability was analyzed by FACS as described previously [12]. In this assay, cells impermeable to PI (propidium iodide; PI negative) are considered as viable. After setting the baseline to exclude cell debris, two populations of PI-permeable (PI positive) dead cells are distinguished based on fluorescence intensity, corresponding to either hypodiploid apoptotic cells or necrotic cells with intact DNA. To define the window of fluorescence associated with normal DNA content, cells are permeabilized with methanol and stained with PI. Here, A20 cells were incubated with either C6 or DH-C6 at concentrations indicated, mostly, however, either 100 μM for 6 h or 50 μM for up to 16 h at 37°C. For inhibition experiments, cells were preincubated for 30 min in either the absence or the presence of the radical scavengers (Trolox 10 mM; Tiron 2 mM), for 3 h with or without catalase (10^4 IU/ml) or for more than 24 h with or without the antioxidant NAC (10 mM). Alternatively, cells were pretreated for 30 min with the poly (ADP-ribosyl) polymerase (PARP) inhibitor 3-ABA at 5 mM. Cells were also treated with the calpain inhibitors E64-D (100 μM) and ALLN 10 μM, as well as inhibitors of autophagy including 3-methyladenine (5 mM), LY294002 (10 μM), or Wortmannin (5 nM). Then either C6 or DH-C6 was added, and cells were incubated for up to 16 h at 37°C. Cells were harvested and stained with 10 μg/ml of propidium iodide to determine cell viability. Samples containing roughly 1×10^4 cells were analyzed by flow cytometry (FACScan, Becton

Dickinson, Mountain View, CA) using the software program FACSDiva.

Protein determination

BCA reagent was used to determine the protein concentration of whole cell lysates according to instructions provided by the manufacturer.

Intracellular calcium measurements

Changes in intracellular calcium concentrations were detected using the fluorescent calcium indicator Fluo-3/AM. A20 cells in suspension (1.0×10^6 cells/ml) were loaded with 5 μM Fluo-3/AM for 30 min at 37°C in culture medium. Then cells were washed twice with Ringer solution (155 mM NaCl, 4.5 mM KCl, 2 mM $CaCl_2$, 1 mM $MgCl_2$, and 5 mM Hepes–NaOH; pH 7.4). Changes in fluorescence of the Fluo-3-loaded cell suspension were monitored in a stirred cuvette with a fluorescence spectrophotometer at 526 nm for up to 2 h following C6 (100 μM) addition.

Lactate dehydrogenase

Supernatant and intracellular lactate dehydrogenase (LDH) concentrations were determined essentially using the CitoTox 96 kit following instructions provided by the manufacturer with minor modifications. Released LDH was standardized to total cellular protein content and expressed as a percentage of total cellular LDH activity (100%).

Electron spin resonance (ESR)

The paramagnetic compound, 5,5-dimethyl-1-pyrroline-*N*-oxide (DMPO, 200 μM) was employed as a spin trap to generate relatively stable adducts with radicals that were then characterized using conventional ESR as described [13]. Signal intensity is a measure of the quantity of adduct formed, while the coupling constants between peaks are indicative of the nature of the short-lived radicals that form an adduct with DMPO. Cells were preincubated for 30 min either in the absence or presence of the radical scavengers (Trolox 10 mM; Tiron 2 mM) or for more than 24 h with or without the antioxidant NAC (10 mM). Then either C6 or DH-C6 was added for 30 min before DMPO was added to the medium for another 10 min. To terminate the experiment the medium was discarded and cells were lysed in a final volume of 500 μl Triton X-100 0.8% (v/v), DMPO 200 mM in DMEM. An aliquot was measured in a capillary tube and the spectra were recorded in the X band (9.85 GHz) using an ESR spectrometer (Bruker ECS 106 spectrometer with a rectangular cavity and 50 kHz field modulation). The hyperfine splitting constants were estimated to be accurate within 0.05 G. To quantify inhibition due to different treatments, heights (h) of the indicated ESR peaks (see boxes) were measured and values obtained were used in the equation:

$$(h_{\mathrm{C6+treatment}} - h_{\mathrm{treatment}})/h_{\mathrm{C6}} - h_{\mathrm{DH}}) \times 100.$$

Flow cytometric assay for ROS production

Scavenger/antioxidant pretreatment (Trolox 10 mM; Tiron 2 mM; NAC 10 mM) followed by C6 treatments was performed as described for viability assays. Dihydrorhodamine 123 (DHR123, 1 μM), a fluorescence probe that is sensitive to oxidative stress, was added to cell suspensions 30 min prior to completing the experiment. After the indicated periods of C6 or DH-C6 exposure, cells were washed with PBS to remove excess probe. The fluorescence of at least 10^4 viable cells was analyzed by flow cytometry.

Determination of intracellular NAD(P)H

A water-soluble tetrazolium salt was used to monitor cellular NAD(P)H levels, as described previously [62]. Cells were seeded in 96-well plates (5×10^5 cells/well) and cultured in 100 μl of medium containing fetal bovine serum and antibiotics for 30 min. Then, C6 (100 μM) was added and cells were cultured further for up to 8 h. At the time points indicated an aqueous mix containing 2-(2-methoxy-4-nitrophenyl)-3-(4-nitrophenyl)-5-(2,4-disulfophenyl)-2*H*-tetrazolium monosodium salt (final conc 5 mM) and 1- methoxy-5-methylphenazinium methylsulfate (final conc 0.2 mM) was added and the resulting absorbance at 490 nm was read up to 4 h later. Reduction of the tetrazolium salt to yield a yellow-colored formazan dye depends essentially on the amount of intracellular NAD(P)H.

Cellular glutathione content

Total cellular GSH was determined using the 5,5′-dithiobis-2-nitrobenzoic acid (DNTB)-dependent recycling assay essentially as previously described [14] and standardized to total protein content. To determine the effect of ceramides, A20 cells (10^6/ml) were treated with 100 μM C6 for 0, 1, 3, or 5 h. Then, cells were washed twice with ice-cold PBS, lysed in a buffer (Tris/HCl 10 mM, pH 7.4, EDTA 5 mM, NaCl 50 mM, Triton X-100 1%, PMSF 1 mM, Na_3VO_4 1 mM), and incubated for 10 min at 37°C. Samples were centrifuged at 13,400×*g* 20 min at 4°C. Trichloroacetic acid (TCA, 2.5% final concentration) was added to the supernatant to precipitate proteins. The pellet obtained after centrifugation was neutralized in 250 mM sodium phosphate buffer (pH 7.4) containing 5 mM EDTA. NADPH in 0.25 M sodium phosphate buffer (pH 7.4) was added, and the absorbance read at different time points using a spectrophotometer (Bio-Tek Instrument Inc, Winooski, VT). GSH content was quantified by comparison with a standard curve. GSH values normalized to total protein content were expressed as a percentage of GSH in nontreated control cells (100%).

Analysis of mitochondrial transmembrane potential

Rhodamine 123, a cationic voltage-sensitive probe that reversibly accumulates in mitochondria [15] was used to detect changes in transmembrane mitochondrial potential. Exponentially growing cells were incubated with C6 or DH-C6 as

indicated in the figure legends. Cells were labeled with 1 μM rhodamine 123 at 37°C in cell medium for 60 min before terminating the experiment. After washing with ice cold PBS, the samples were analyzed by flow cytometry.

Adenovirus-mediated expression of catalase

A20 cells were transduced at multiplicity of infection (MOI) 100,000 with adenovirus catalase (AdCAT) [16] or an empty adenovirus as a control. This MOI was shown in preliminary experiments to yield 100% transduction efficiency. A20 cells (24 h posttransduction) were incubated in complete medium at 37°C with either C6 or DH-C6 at 100 μM for 6 h or 50 μM for up to 16 h at 37°C. Cell viability was analyzed by FACS as described previously. Expression of AdCAT was confirmed 48 h posttransduction by measuring the activity of catalase as previously described [16].

Measurement of ATP

Cellular ATP content was measured using a luminescence assay (Cell-Titer Glo Kit, Promega) following the manufacturers instructions. Briefly, A20 cells were incubated up to 6 h with C6 at the concentrations indicated. For inhibition experiments, cells were preincubated for 30 min in either the absence or the presence of the radical scavenger (Tiron 4 mM) or the PARP inhibitor 3-ABA (5 mM). Final luminescence was measured in a TopCount NXT microplate luminescence counter (Perkin-Elmer, Waltham, MA).

Data analysis

Data sets were compared using nonparametric Kruskall-Wallis analysis. Comparisons yielding $P=0.05$ or less were considered indicative of statistically significant differences.

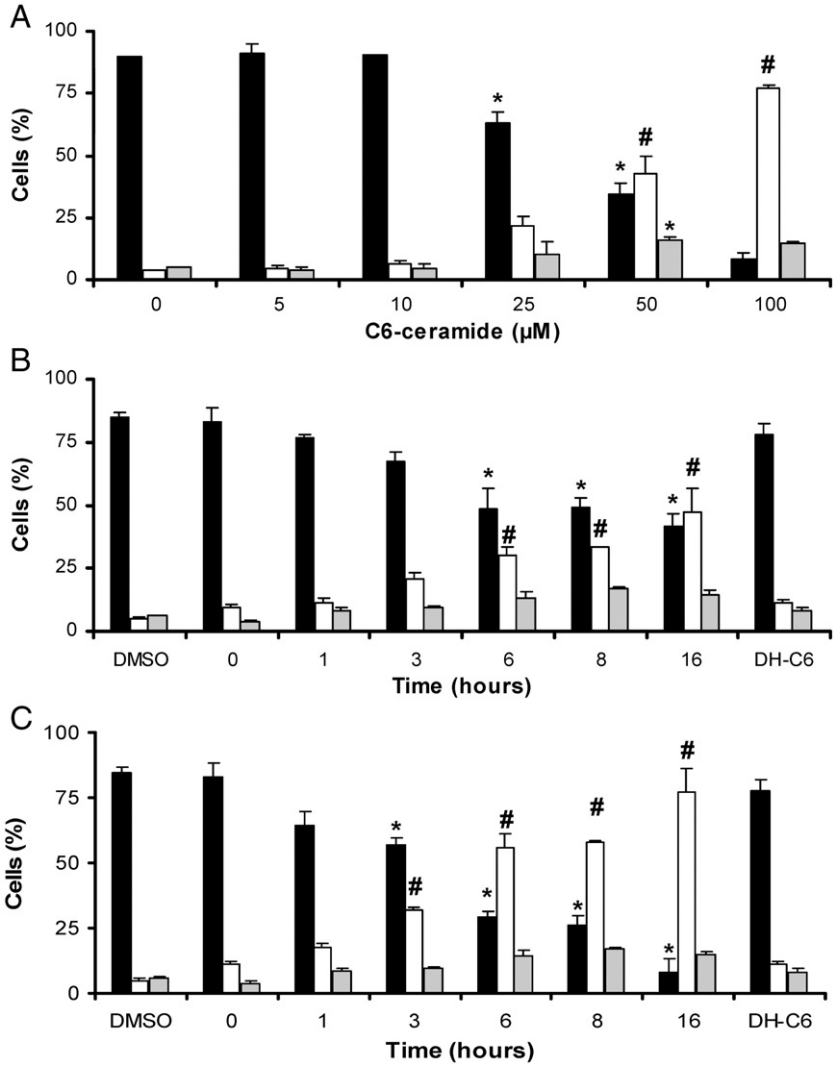

Fig. 1. A20 cell death in response to C6 treatment: dose and time dependence. (A) A20 cells were treated with various concentrations of C6 (C6, up to 100 μM) or the DMSO solvent control (concentration 0 μM). After 16 h, cell death by apoptosis and necrosis was quantified by FACS analysis following PI staining as described under Methods. Using the C6 concentrations of 50 μM (B) or 100 μM (C), progression of apoptotic and necrotic cell death over time (h) was assessed. Cell viability (black bars) and cell death by either necrosis (white bars) or apoptosis (gray bars) are depicted. Values shown are the mean±SD of three independent experiments in duplicate. Statistically significant decreases in viability (*$P=0.005$) and increases in cell necrosis (#$P=0.005$) are indicated.

Results

Previous results from this laboratory implicated ceramide as a mediator of nonapoptotic cell death downstream of the Fas receptor. Specifically, this alternative caspase-8-dependent, but caspase-3-independent cell death mode observed in lymphocytes, was defined as necrosis based on the observations that cell membranes of this subpopulation became PI permeable in the absence of DNA laddering or nuclear fragmentation and cell volume increased. Similar changes were induced by addition of short-chain, cell-permeable ceramides to the culture medium [12]. Here we investigated potential signaling mechanisms implicated in ceramide-mediated cell death using C6, the A20 mouse B lymphoma, and Jurkat T cell models as well as a previously characterized flow cytometry assay to rapidly identify and quantify the necrotic cell population [12].

Cell death after 16 h in response to addition of C6 at different concentrations was dose dependent (Fig. 1A). Significant reductions in cell viability were already apparent at 25 μM concentrations and cell death beyond 50% was observed in the presence of 50 μM or more C6. As previously reported [12], cell death was predominantly necrotic by nature while only modest increments in the number of apoptotic cells (up to 15%) were detected by this assay. In the presence of DH-C6, a commonly used negative control, no significant increments in cell death were detected at the same concentrations (see Figs. 1B and 1C). Time dependence of the two cell death modes was established using C6 at 50 and 100 μM (Figs. 1B and 1C, respectively). Approximately 50% necrosis was detected with either C6 concentration after 16 and 6 h incubation, respectively. Both of these conditions were employed in most of the following experiments. Results obtained using 100 μM for 6 h are predominantly shown.

A large number of putative downstream effectors of ceramide have been described in the literature (see Introduction). However, in light of more recent evidence associating particularly the formation of ROS with regulated forms of necrotic cell death (10 and references therein) we became interested in pursuing the hypothesis that intracellular ROS generated on cell treatment with permeable ceramides might represent a causative agent that leads to necrotic cell death.

To directly monitor the kinetics of ROS formation, dihydrorhodamine 123 (DHR123), a fluorescent probe that is sensitive to oxidative stress, was employed. In DHR123-loaded A20 cells (Fig. 2), C6 (50–100 μM) induced significant (2- to 4-fold) increases in DHR123 fluorescence within 30 min that were not observed with DH-C6 (Fig. 2A). A20 cells were then pretreated with either Trolox, a vitamin E analog, Tiron, a superoxide scavenger, or the antioxidant NAC before incubating with 50 or 100 μM C6 for 6 h (Fig. 2B). Interestingly, both Tiron (2 mM) and NAC (10 mM), but not Trolox (10 mM), substantially reduced fluorescence increments triggered after 30 min by either 50 or 100 μM C6 (Fig. 2B).

These results indicated that C6-induced ROS formation occurred rapidly within 30 min to 1 h following ceramide administration. To corroborate these findings, an alternative approach involving trapping of ROS species in a more stable

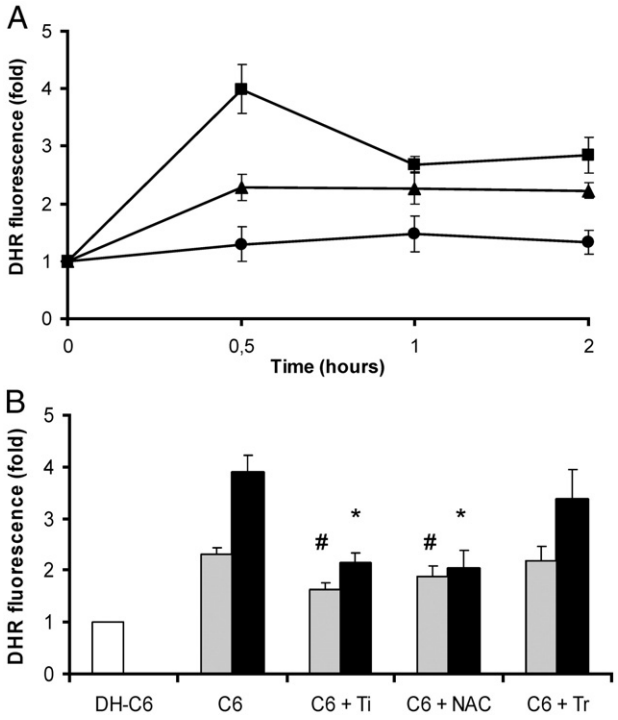

Fig. 2. Generation of ROS by C6 in A20 cells. (A) C6-induced changes in dihydrorhodamine 123 (DHR123) fluorescence were quantified as a measure of ROS formation. Changes relative to the basal fluorescence value (defined as 1) are indicated for 50 (black triangles) or 100 μM (black squares) C6 or 100 μM DH-C6 (black circles). (B) A20 cells were pretreated with 2 mM Tiron (Ti) or 10 mM Trolox (Tr) for 30 min or NAC (10 mM) for 24 h. Then cells were incubated with 50 μM (gray bars) or 100 μM (black bars) of C6 for 30 min after which DHR123 fluorescence was determined. As a control, cells were incubated with the corresponding concentrations (50 or 100 μM) of DH-C6 (white bar) and fluorescence values measured here in the absence of antioxidants were assigned the value 1. Values shown are the mean ± SD of six independent experiments in duplicate. Statistically significant reductions in C6-induced DHR123 fluorescence were detected on preincubation with either Tiron or NAC (*P=0.01; #P=0.05) but not Trolox.

adduct with DMPO and subsequent analysis by ESR was included (Fig. 3, upper panels). After 30 min in the presence of C6 or DH-C6, DMPO was added and the samples were processed as described. The spectra obtained revealed peaks characteristic of a DMPO-ROS adduct only when cells had been exposed to C6, but not with DH-C6. Furthermore, pretreatment of cells with Tiron (2 mM) prevented C6-induced ROS formation, as evidenced by the absence of the DMPO-ROS adduct in the ESR spectrum. The extent to which preincubation with Tiron was able to quench ceramide-induced ROS formation was also assessed numerically and compared with the effectiveness of other compounds including NAC and Trolox (table, Fig. 3). As expected from the previous data, NAC was as effective as Tiron at blocking ROS formation, while Trolox essentially had no effect.

To associate ROS formation with ceramide-induced cell death, the effects of ROS scavengers and antioxidants on ceramide-induced cell death were evaluated (Fig. 4A). As in previous experiments, C6 induced a 40–50% reduction in cell viability compared to controls or cells incubated with the same concentration of DH-C6. Pretreatment with Trolox (10 μM) was

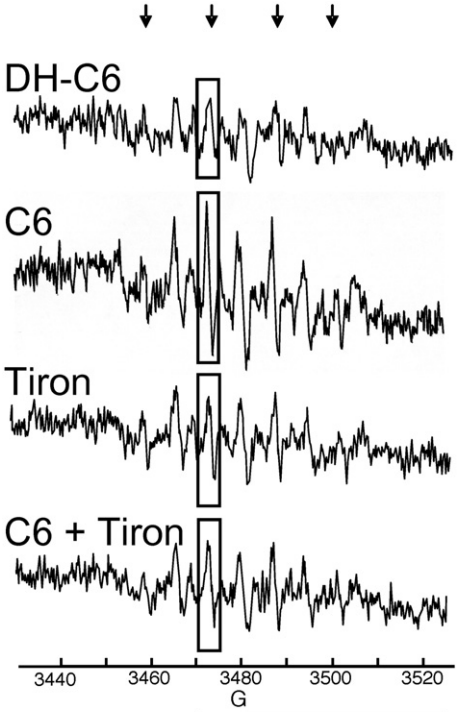

	Inhibition (%)
C6	0
C6 + Tiron	90 +/- 4
C6 + Trolox	10 +/- 1
C6 + NAC	85 +/- 5

Fig. 3. Identification of C6-induced ROS formation by ESR analysis. A20 cells (2.5×10^5/ml) were treated with 100 μM C6 or DH-C6 for 30 min. DMPO (200 mM), C6, or DH-C6 was added at the same time. In protection experiments, cells were preincubated with Trolox (10 mM) or Tiron (2 mM) for 30 min or NAC (10 mM) for 24 h and then analyzed following incubation for an additional 30 min in the absence or presence of C6. The peaks highlighted by a rectangular box in the spectra were employed to calculate inhibition data as described. Arrows indicate spin adducts of hydroxyl and superoxide species. Other peaks are unknown radicals, probably due to DMPO decomposition. Representative ESR spectra obtained using ceramide together with Tiron are specifically shown here (upper panels). Results from experiments also including NAC and Trolox are summarized in the table (lower section of figure). Values shown are the mean±SD of three independent experiments in duplicate.

unable to revert ceramide-induced cell death, while significant protection was observed using either Tiron (2 mM) or NAC (10 mM). Similar results were also obtained when preincubations were followed by the addition of 50 μM C6 for 16 h (data not shown).

As an additional, independent approach to implicate ceramide-induced ROS formation as crucial in promoting necrosis, A20 cells were transduced with either empty adenovirus or adenovirus encoding catalase [16]. Successful expression of catalase was verified by measuring activity in cell extracts. On an average, significant 3-fold increases in activity were observed following adenovirus-mediated catalase expression but not with the empty virus (data not shown). As expected based on the previous findings, increased catalase activity correlated with improved cell viability and reduced cell necrosis in C6-treated A20 cells, while no changes for apoptosis were detectable in the same experiments (Fig. 4B).

Results so far showed that ceramide-induced ROS formation was a relatively rapid event that was blocked by NAC and Tiron, but not Trolox. Likewise, ceramide-induced necrotic cell death was effectively quenched by the former two reagents but not the latter, implicating ROS formation as a causative link to onset of necrotic cell death. This was substantiated in experiments showing protection of A20 cells from C6-induced necrosis on adenovirus-mediated catalase expression.

Nonetheless, a considerable temporal discrepancy was apparent between the time points at which ROS formation was detected (30 min to 1 h) and at which death was quantified in our assays (generally after 6–16 h). Hence we sought to define the point at which ceramide- and potentially ROS-induced damage to cells became irreversible. To that end, cells

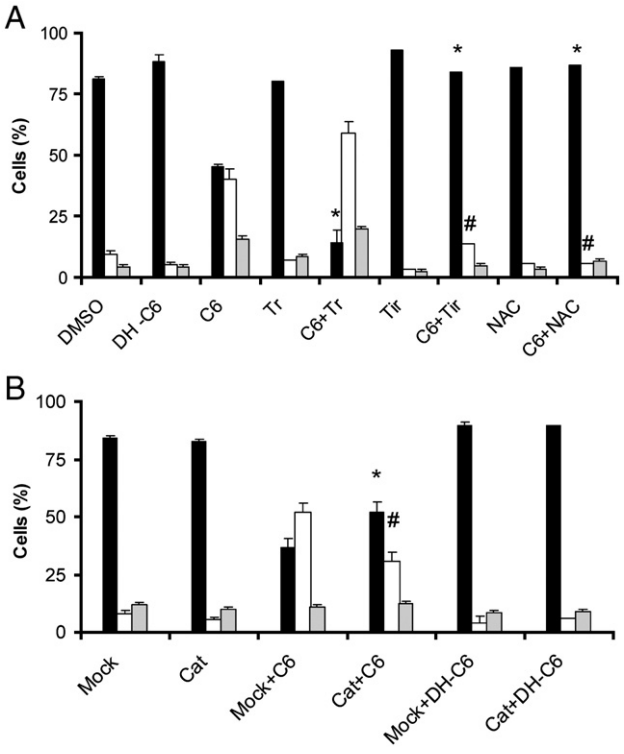

Fig. 4. Effects of ROS scavengers and antioxidants on C6-induced A20 cell death. (A) A20 cells were pretreated with either Trolox (Tr, 10 mM) or Tiron (Tir, 2 mM) for 30 min or NAC (10 mM) for 24 h. Following preincubation, the medium was replaced by medium containing 100 μM C6. As controls either DMSO or DH-C6 was employed. Cell viability (black bars) and death by necrosis (white bars) and apoptosis (gray bars) were determined after 6 h by flow cytometric analysis following PI staining. Statistically significant changes in viability (*P=0.01) and in cell necrosis (#P=0.01) due to A20 cell pretreatment are indicated. (B) A20 cells were transiently transduced with either empty adenovirus (Mock) or adenovirus harboring a cDNA for catalase expression (Cat). Cells were then either treated for 16 h with 100 μM C6 or DH-C6 or left untreated. Cell viability (black bars), as well as cell death by necrosis (white bars) and apoptosis (gray bars), was quantified by flow cytometric analysis following PI staining. Values shown are the mean±SD of three independent experiments in duplicate. Statistically significant increases in cell viability (*P=0.05) and decreases in necrotic cell death (#P=0.05) due to catalase expression are indicated.

incubated for time periods up to 4 h with C6, after which the ceramide-containing medium was replaced by fresh ceramide-free medium, were compared with cells treated with C6 for 16 h (Fig. 5). Interestingly, apoptotic cell death was irreversibly induced at an earlier time point (after 2–3 h) than necrotic cell death (after 3–4 h). However, while apoptosis essentially reached a plateau of 20–30% within the first 3 h, induction of necrosis required exposure to C6 beyond 3 h to become readily detectable and increased on exposure for 16 h. The distinct kinetics are indicative of different underlying mechanisms and suggest that irreversible changes associated with ceramide-induced necrosis occur after 3 h of exposure to the reagent.

Necrosis is associated with cell swelling, membrane rupture, and release of cytosolic contents to the environment, whereby loss of membrane integrity is considered an early event in the process. Precisely this trait is an important factor held responsible for the dramatic differences in responses of the immune system to cell death by either apoptosis or necrosis. Thus, C6-induced release of cytosolic contents was characterized by measuring the accumulation of LDH activity in the medium for short time periods up to 6 h. (Fig. 5C). As expected, based on the initial results (Figs. 1B and 1C), increments in LDH activity became significant within 1–3 h following addition of C6, whereby release was more rapid in the presence of 100 μM C6 (Fig. 5C). For both C6 concentrations, increments in PI-positive cell populations detected by the flow cytometry assay (Figs. 1B and 1C; 50 and 100 μM, respectively) matched the kinetics of LDH release (Fig. 5C). Surprisingly, although plasma membrane permeability increased significantly within the initial 3 h of ceramide exposure by both criteria, this change did not correlate with an increase in necrotic cell death observed after 16 h (see Fig. 5B). These observations may be taken to suggest that early damage at the plasma membrane was not necessarily the cause of necrotic cell death later on; however, alternative explanations for these results cannot be excluded.

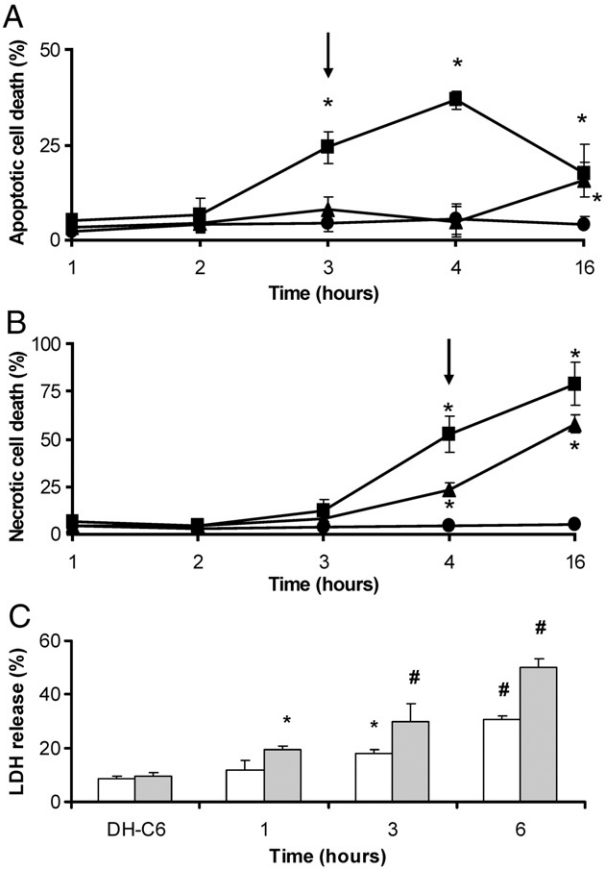

Fig. 5. Reversibility of C6-induced death in A20 cells. A20 (2×10^6/ml) cells were incubated with 50 (black triangles) or 100 μM (black squares) C6, or DH-C6 (black circles) for the time points up to 4 h. Then ceramide-containing medium was replaced by fresh medium without C6 and cell culture was continued to 16 h. Alternatively, cells were maintained in medium with C6 or DH-C6 for the entire 16 h period. Then cell death by apoptosis (A) or necrosis (B) was determined by the flow cytometric assay following PI staining. Statistically significant increments in cell death (*$P=0.001$) are indicated. (C) LDH activity measured in supernatants after cell treatment with 50 (white bars) or 100 μM (gray bars) C6 was standardized to total LDH activity observed on cell lysis in the presence of 1% Triton X-100 (100%). A20 cells treated for 6 h with the same concentrations of DH-C6 were employed as controls. Values shown are the mean±SD of three independent experiments in duplicate. Statistically significant increments in LDH release (*$P=0.05$; #$P=0.005$) are indicated.

Given that NAC and Tiron pretreatment efficiently precluded ceramide-induced necrosis, we investigated whether induction of necrosis may be linked to ROS-mediated depletion of intracellular GSH levels (Fig. 6A). Indeed, depletion of GSH became significant after 3–4 h of C6 exposure, suggesting that GSH depletion might be linked to the induction of changes required for necrosis.

The results so far indicated that the source of ROS was probably located in the cytosol rather than at the plasma membrane. Given that ceramide-induced changes in the mitochondria have been reported previously [17–20] and the fact that mitochondrial represent a major potential source of ROS in the cell, the possibility that cell-permeable ceramides might alter mitochondria function was assessed. Rhodamine, a dye that augments fluorescence on incorporation into the membrane of intact mitochondria, was employed to track changes in mitochondrial function, since fluorescence of the dye decreases as mitochondrial membrane potential is lost [4,5,15]. Indeed, small changes in fluorescence were detectable within 1 h of incubation with C6 (100 μM) and increased subsequently in a time-dependent fashion. Decreases in fluorescence by roughly 50% were apparent after 4 h (Fig. 6B). Thus, ceramide-induced loss of mitochondrial membrane potential correlated well with onset of ROS formation (see Fig. 2B). However, while ceramide-induced mitochondrial damage correlated well with ROS formation, these organelles did not appear to represent prime targets of subsequent ROS-induced damage, since preincubation with NAC or Tiron did not alter the progression of changes in mitochondrial membrane potential (Fig. 6C).

ATP is essential for apoptotic cell death and although ATP does decline, levels are maintained to an extent that permits execution of the process. Necrosis, however, is characterized by a precipitous drop in ATP and once below 25% of the steady-state levels, cell death via necrosis is thought to be irreversible. Given the potentially pivotal role attributed to ATP in this

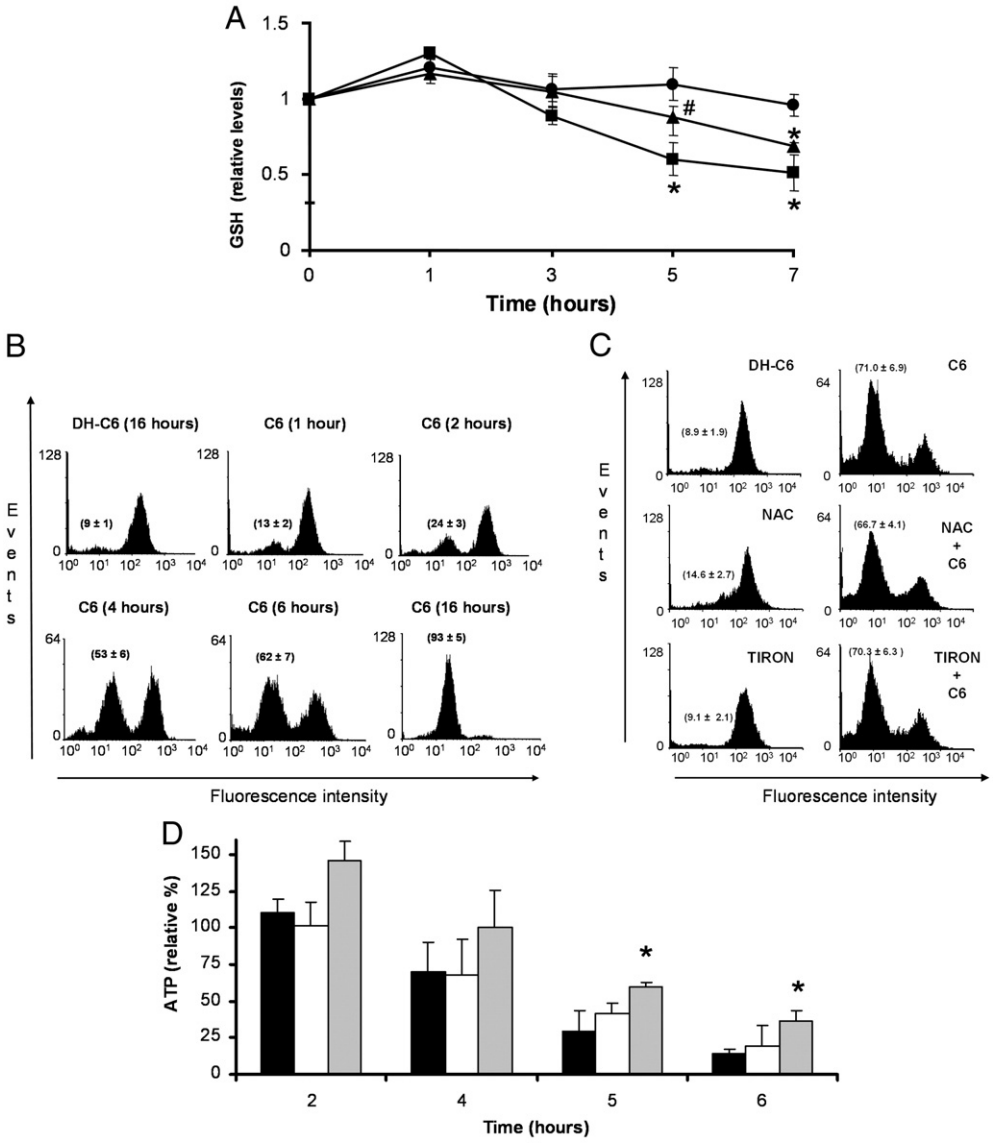

Fig. 6. C6-induced changes in GSH, mitochondrial transmembrane potential, and ATP of A20 cells. (A) A20 (2×10^6/ml) cells were incubated with 50 (black triangles) or 100 μM (black squares) C6, or DH-C6 (black circles) for the time points indicated up to 7 h. At the end of the treatment, cells were washed twice with ice-cold PBS and total glutathione (GSH) content was analyzed as described under Methods. Data indicate the relative changes in GSH content whereby the mean GSH content per milligram of cellular protein (12.5 nmol/mg) in the absence of treatment was defined as 100%. Statistically significant reductions in GSH (*$P=0.005$; #$P=0.01$) are indicated. (B) A20 cells were incubated with 100 μM C6 or DH-C6 for up to 16 h. To identify changes in the mitochondrial transmembrane potential, cells were labeled with rhodamine 123 (1 μM final concentration), 1 h before terminating the experiment. At the indicated time points cells were washed in PBS to remove excess probe and rhodamine 123 fluorescence was analyzed by FACS as described. Values averaged from these experiments ($N=3$) are shown in brackets. (C) A20 cells were pretreated with either NAC (10 mM) for 24 h or Tiron (2 mM) for 30 min. Following preincubation, the medium was replaced by medium containing 100 μM DH-C6 or C6 and incubation was continued for another 6 h. The mitochondrial transmembrane potential was analyzed by FACS, as noted before using the fluorescent dye rhodamine 123 added 1 h before terminating the experiment. Values averaged from these experiments ($N=3$) are shown in brackets (mean±SD). (D) ATP levels were measured in A20 cells following exposure to 100 μM C6 (black bars) and with 100 μM C6 after pretreatment with 5 mM 3-ABA (white bars) or 4 mM Tiron (gray bars) for the indicated periods of time. Values shown (D) are the mean±SD of six independent experiments in duplicate. Statistically significant delays in ATP reduction (*$P=0.05$) are indicated.

context, we measured cellular ATP levels following ceramide treatment. Indeed, ceramide-induced decreases in ATP were particularly pronounced after roughly 4 h of exposure to the reagent (Fig. 6D, black bars).

Our previous studies indicated that ceramide-induced necrosis downstream of the Fas-receptor also occurred in Jurkat T cells. Hence, the observations in A20 cells were corroborated in this alternative cell model (Fig. 7). Jurkat T cells were found to be more sensitive to C6 in that greater declines in viability and increased cell necrosis were observed using the standard conditions for A20 cells, 50 μM (16 h) and 100 μM (6 h) (Fig. 7A). Nonetheless, both NAC and Tiron, but not Trolox, protected Jurkat cells from ceramide-induced necrosis (Fig. 7C) and ablated ceramide-induced ROS formation (Fig. 7B and data not shown). Coincident with elevated sensitivity to C6, the kinetics of loss of mitochondrial membrane potential were more rapid for

Jurkat T cells with a 60% decline in rhodamine 123 fluorescence after 2 h and 70% less after 6 h (Fig. 7D). Also, a precipitous decrease in cellular ATP levels was detectable within roughly the same time frame up to 6 h (Fig. 7E, black bars). Taken together, the data indicate that necrosis induced by C6 in Jurkat T cells occurs via mechanisms similar if not identical to those in A20 B cells.

As an alternative, we evaluated the possibility that ROS-induced activation of PARP may provide the missing link to ceramide-induced necrosis, since uncontrolled PARP activity consumes enormous amounts of ATP and is frequently associated with necrosis [21,22]. However, the PARP inhibitor 3-ABA did not delay in a statistically significant manner ceramide-induced decreases in ATP levels in either A20 (Fig. 6D, white bars) or Jurkat T (Fig. 7E, white bars) cells. Likewise ceramide-induced necrosis after 6 h was not modulated by the presence of 3-ABA in either cell line (data not shown). In contrast, hydrogen peroxide-induced ATP depletion and necrosis were both blocked by 3-ABA pretreatment in Jurkat T cells (Figs. 8A and 8B) and A20 cells (data not shown). Importantly, pretreatment of A20 and Jurkat T cells with the radical scavenger Tiron (4 mM) offered significant protection from ATP depletion (see Figs. 6D and 7E, gray bars, for A20 and Jurkat T cells, respectively). Somewhat surprisingly, however, despite inhibition of PARP, NAD(P)H levels declined in a manner similar to those of ATP in the presence of 3-ABA (see Figs. 8C and 8D). Thus, NAD(P)H consumption in a manner independent of PARP activation may contribute to onset of necrotic cell death. Taken together, these data indicate that ceramide-induced ROS formation, probably as a consequence of mitochondrial damage, results in precipitous ATP decline and necrosis in lymphoid cells that appears not to be linked to PARP overactivation, but may involve NAD(P)H consumption by alternative mechanisms.

Discussion

A considerable body of evidence implicates ceramides in apoptotic cell death [1,23,24]. More recently, however, several reports indicate that cell death with necrotic features may occur as a consequence of increased endogenous ceramide levels, as well as in response to treatment with cell-permeable ceramides [12,25–28]. Here it is important to note that necrotic cell death has been identified as a regulated process and defined accordingly necrosis-like PCD, thereby emphasizing the active nature of the process and in doing so distinguishing it from accidental necrosis, a passive process [10,11].

Our previous studies showed that signaling via Fas leads to both apoptotic and necrotic cell death in A20 B-lymphoma and Jurkat T cells, but not in Raji B cells where lipid scrambling and ceramide production are blocked. In addition, delayed endogenous ceramide production was observed in A20 cells and linked specifically to FasL-induced necrosis. Furthermore, addition of exogenous cell-permeable C2 and C6 leads to predominantly necrotic cell death in A20, Jurkat, and Raji cells [12]. In this study, we sought to define the mechanism(s) by which cell-permeable ceramides promote cell necrosis.

Our previous and current studies relied heavily on the use of a flow cytometric assay that identifies the different dead cell populations on the basis of fluorescence intensity due to DNA staining by PI that entered the cell as a consequence of augmented membrane permeability [12]. In order to evaluate whether A20 membrane permeability to PI triggered by exposure to cell-permeable ceramides correlated with release of cytoplasmic content from cells, LDH release, a criteria frequently employed to identify necrotic cell death, was compared with results obtained in parallel using the flow cytometric assay. As expected, ceramide-induced necrosis observed in A20 cells using the flow cytometric assay (Figs. 1A and 1B) correlated well with LDH liberation determined in the first 1–6 h of ceramide treatment (Fig. 5C). Thus, cell-permeable C2 (data not shown) and C6, but not the respective DH-C6 compounds, rapidly augment cell membrane permeability and release of cytosolic components. Consistent with the notion that major changes occur at the plasma membrane, ceramide production has been shown to contribute to cell death by promoting reorganization of the plasma membrane and fusion of lipid rafts [29]. Furthermore, cell-permeable ceramides are known to form pores in artificial membranes [17,18,30].

Rather intriguingly, however, despite release of LDH within the first 2–3 h (Fig. 5C), damage to A20 cells was largely reversible if they were transferred back to medium without ceramide within this period (Figs. 5A and 5B). Recovery following exposure to 50 μM C6 for 3 h or 100 μM C6 for 2 h was complete. Thereafter, a modest degree of apoptosis was observed with 100 μM C6 while increasing necrosis became apparent for both C6 concentrations. These results indicate that permeability of the plasma membrane detected at early time points by measuring both PI and LDH permeability was neither the primary cause of nor strictly linked to cell death observed later on. In A20 cells, the ability to recover was maintained for a limited period of time (roughly 3 h). Decreases in intracellular GSH stores (Fig. 6A), observed in response to C6, became significant after about 3 h and coincided with a pronounced

Fig. 7. Effects of C6 in Jurkat T cells. Experiments described for A20 cells were repeated in Jurkat T cells. (A) Jurkat T cells were incubated with either 50 or 100 μM C6 for 16 h and viability (black bars) and cell death by necrosis (white bars) or apoptosis (gray bars) were determined by the flow cytometric assay following PI staining. Statistically significant decreases in cell viability ($^{*}P=0.01$) and increases in necrosis (#$P=0{,}001$) are indicated. (B) ROS formation in Jurkat T cells was determined using DHR123 for cells treated with 50 μM (black triangles), 100 μM (black squares) C6, or 100 μM DH-C6 (black circles) at the time points indicated up to 2 h as described (see Fig. 2). (C) Viability and cell death in Jurkat T cells preincubated with Tiron, Trolox, or NAC and then treated with 100 μM C6 for 6 h were determined as described in Fig. 4. Statistically significant increments in viability ($^{*}P=0.05$) and reductions in cell necrosis (#$P=0.05$) due to pretreatment with antioxidants are also indicated. (D) Alterations in mitochondrial membrane potential observed using rhodamine 123 in Jurkat T cells following treatment for 6 h with 100 μM C6 or 100 μM DH-C6 were determined as described (see Fig. 6). (E) ATP levels were measured in Jurkat cells following exposure to 100 μM C6 (black bars) or 100 μM C6 after pretreatment with either 5 mM 3-ABA (white bars) or 4 mM Tiron (gray bars) for the indicated periods of time. Statistically significant delays in ATP reduction ($^{*}P=0.05$) are indicated. Values shown are the mean ± SD of three (A, B, C, E) or four (D) independent experiments in duplicate.

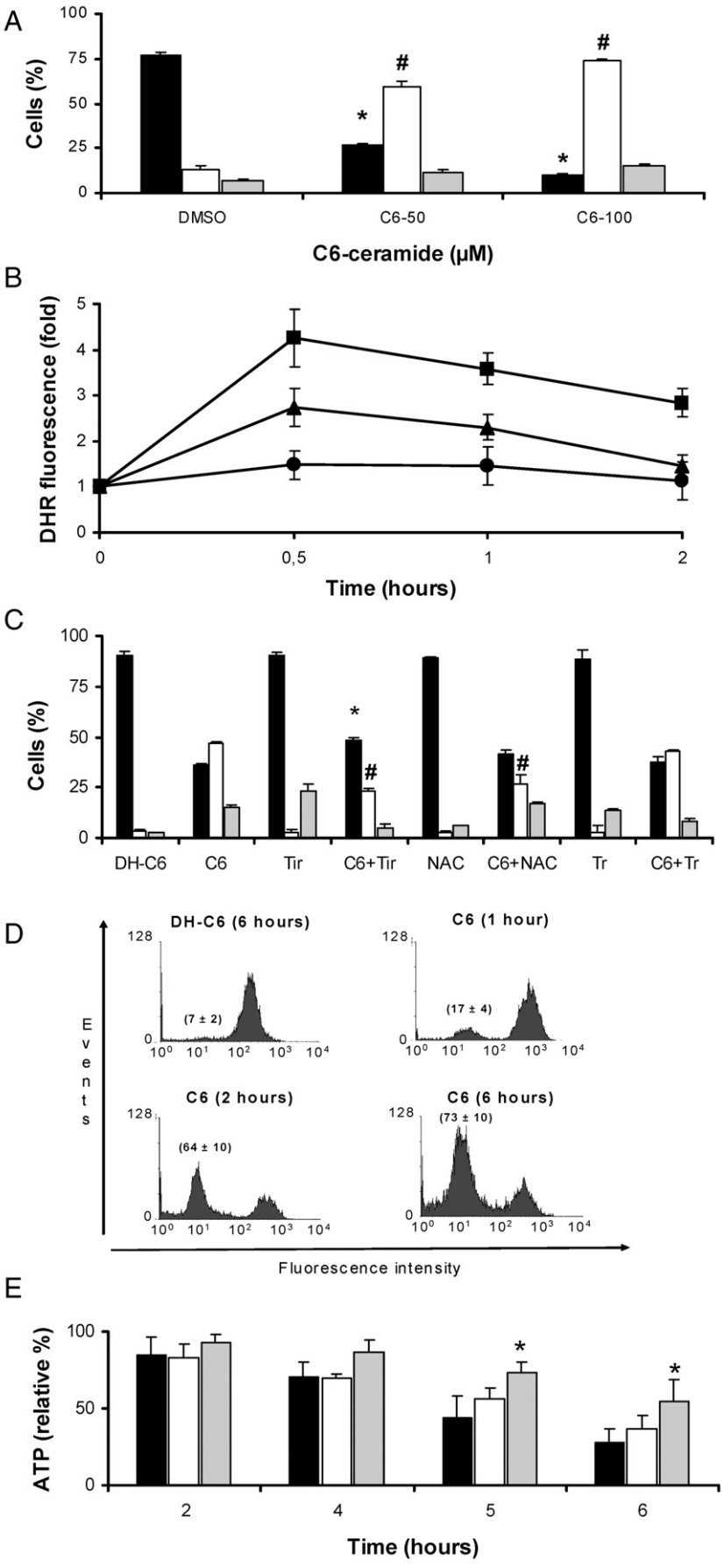
A
Cells (%)
100
75
50
25
0
DMSO
C6-50
C6-100
C6-ceramide (μM)
B
DHR fluorescence (fold)
5
4
3
2
1
0
0
0,5
1
2
Time (hours)
C
Cells (%)
DH-C6
C6
Tir
C6+Tir
NAC
C6+NAC
Tr
C6+Tr
D
DH-C6 (6 hours)
(7 ± 2)
C6 (1 hour)
(17 ± 4)
C6 (2 hours)
(64 ± 10)
C6 (6 hours)
(73 ± 10)
Events
Fluorescence intensity
E
ATP (relative %)
2
4
5
6
Time (hours)

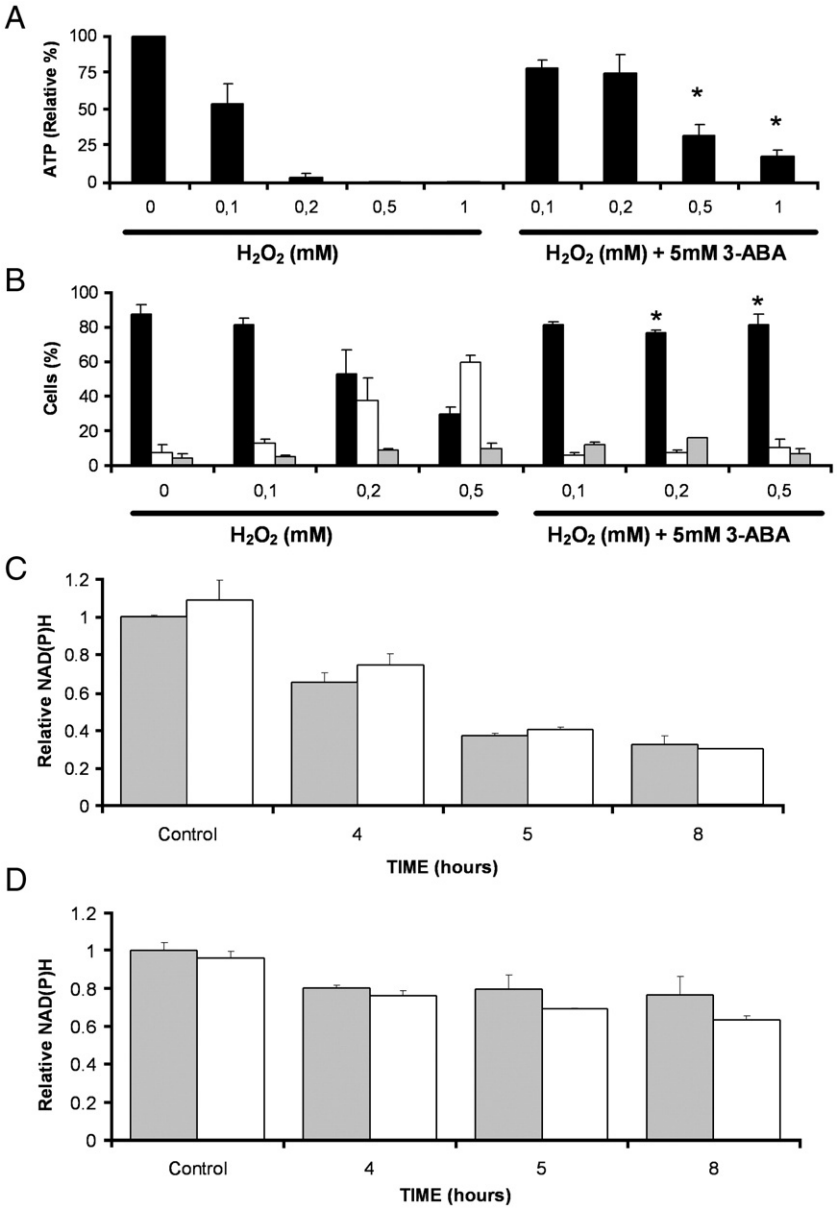

Fig. 8. Hydrogen peroxide-induced ATP decline and necrosis were blocked by the PARP inhibitor 3-ABA. (A) ATP levels were measured after 6 h in Jurkat T cells following treatment with the indicated H_2O_2 concentrations in the absence or presence of 3-ABA (5 mM). (B) Cell viability and death following H_2O_2 treatment in the absence or presence of 3-ABA (5 mM) after 6 h in Jurkat T cells. Cell viability (black bars) and cell death by either necrosis (white bars) or apoptosis (gray bars) are depicted. Values shown (A, B) are the mean±SD of four independent experiments in duplicate. Statistically significant increments in ATP (A) and viability (B) due to the presence of 3-ABA are indicated (*P=0.01). Additionally, NAD(P)H levels were measured and expressed relative to basal values in the absence (gray bars) or presence of 3-ABA (5 mM) during the first 8 h of exposure to C6 (100 μM) in A20 cells (C) and Jurkat cells (D). Values shown (C, D) are the mean±SD of three independent experiments in duplicate. No statistically significant differences due to the presence of 3-ABA were detected.

decrease in ATP levels (Fig. 6C). These observations indicate that a considerable lag exists between onset of membrane alterations (rapid) and intracellular events linked to execution of an alternative cell death program. Consistent with this interpretation, pretreatment with NAC, a precursor of GSH, protected A20 cells against ceramide-induced necrotic but not apoptotic cell death (Fig. 4A). Taken together, the data favor the interpretation that ceramide-induced effects at a site (organelle) other than the plasma membrane are responsible for triggering necrotic cell death.

A large body of literature is available linking intracellular formation of reactive oxygen species to cell death by apoptosis [31–33] or necrosis [9,34–36]. Furthermore, ROS formation is also associated with simultaneous activation of pathways leading to necrotic and apoptotic death in the same cells [12,37–39]. Interestingly, low levels of oxidative stress favor apoptosis while excessive oxidative stress precludes caspase activation and drives cells toward necrosis [38,40]. Given these data, we investigated whether ROS formation might be linked to cell death mediated by cell-permeable ceramides. Indeed, ceramide

rapidly induced an increase in ROS formation within 30–60 min (Fig. 2A) that was blocked by some but not all treatments with antioxidants or scavengers (Fig. 2B). In particular, reagents thought to modulate predominantly the redox environment of the cytosol, like Tiron and NAC, efficiently reduced detectable ROS formation (Fig. 2B). Alternatively, the vitamin E analog Trolox that preferentially offers protection at the plasma membrane was essentially ineffective (Fig. 2B). Also, NAC and Tiron, but not Trolox, provided statistically significant protection against ceramide-induced necrosis but not apoptosis (Fig. 4A). The presence of catalase in the culture medium (10^4 U/ml) at concentrations that ablate effects observed as a consequence of H_2O_2 formation via the plasma membrane-associated NADPH oxidase complex in HTC cells [41] was unable to protect A20 cells from ceramide-induced death (data not shown). Alternatively, however, intracellular expression of catalase in A20 cells using adenovirus-mediated transduction reduced significantly ceramide-induced necrosis (Fig. 4B). Our findings are entirely consistent with numerous reports that document the ability of catalase to preclude cell death in response to various stimuli ranging from xenobiotics to cytokines [8]. Most importantly, the data indicate that C6-mediated alterations at an intracellular site, rather than the plasma membrane, and, as a consequence of ROS, may be responsible for triggering necrotic cell death.

Mitochondria are the major oxygen-consuming as well as ROS-forming organelles of a cell. In healthy cells, some 2% of the oxygen consumed by mitochondria is converted into ROS. Furthermore, even modest impediments to normal mitochondrial function are known to augment oxidative uncoupling and ROS formation and initiate damage to the cellular as well as mitochondrial environment. The major species generated as a consequence of mitochondrial malfunction are hydroxyl and superoxide radicals. Our analysis using dihydrorhodamine indicated that ROS species became rapidly detectable within 30 min in the A20 and Jurkat cells in response to ceramide treatment (Figs. 2A and 7B). This increment was significantly reduced by those antioxidants that protected against ceramide-induced cell death, NAC and Tiron, but not Trolox (compare Figs. 2B, 3, and 4A). Likewise, ESR experiments with the spin-trap DMPO indicated that hydroxyl radicals were being generated (Fig. 3). Taken together, these results pointed toward mitochondria as a possible source of ROS that contribute to necrosis. Consistent with this notion, rapid decreases in mitochondrial membrane potential were detected in A20 and Jurkat cells following incubation with cell-permeable ceramides (Figs. 6B and 7D).

Several studies have demonstrated strong links between ceramide and mitochondria in the regulation of apoptosis (for a review, see [42]). Ceramide leads to inhibition of the mitochondrial respiratory chain complex III [4]. Also, mitochondrial targeting of bSMase (bacterial sphingomyelinase) induced ceramide accumulation in mitochondria that was sufficient to promote apoptosis [20]. Furthermore, ceramide-metabolizing enzymes have been localized to mitochondria [43,44] and trafficking of glycosphingolipids from the plasma membrane to mitochondria has been associated with cell death [45]. Finally, recent studies suggest that ceramide could interact with elements of the mitochondrial apoptotic machinery, in particular Bax [46]. Interestingly, administration of cell-permeable ceramides also leads to increments in endogenous ceramide levels by promoting ceramide biosynthesis [47]. These data from the literature point toward mitochondria as either direct or indirect targets of cell-permeable ceramides. Our findings are entirely consistent with this interpretation.

The mitochondrial permeability transition (MPT) is thought to represent a critical determinant in the execution of apoptosis, necrosis, and other forms of cell death (for review, see [48,49]). Limited MPT resulting from milder mitochondrial damage is proposed to leave the cell with sufficient energy for ATP-dependent autophagic and apoptotic PCD. Alternatively, however, MPT in the vast majority of mitochondria following extensive mitochondrial damage and uncoupling of oxidative phosphorylation stimulates a necrotic response (for review, see [50]). Such uncoupling was suggested by Lemasters et al. [49] to result in ROS production, as well as uncontrolled hydrolysis of ATP by the inner membrane ATPase. Hence, modification of intracellular ATP concentrations may serve as one possible mechanism permitting the switch from apoptotic to necrotic cell death [51].

Clearly, exposure to cell-permeable ceramides triggers predominantly necrosis, although some apoptosis is also detected (Fig. 1). The early changes in mitochondrial membrane potential observed on treatment of both A20 and Jurkat cells with C6 (Figs. 6B and 7D) make the mitochondria likely targets of these reagents.

Although a temporal correlation between ROS formation and mitochondrial malfunction existed at the onset (compare Figs. 2A and 7B with Figs. 6B and 7D), this did not prevail over time. ROS detected using dihydrorhodamine reached a plateau while mitochondrial depolarization continued. On the one hand, these results likely reflect the ability of the cell cytosol and mitochondrial matrix to rapidly quench ROS increases until the total intracellular reductive capacity has been surpassed. Consistent with this interpretation, significant decreases in GSH levels were only apparent 3 h after ceramide addition (Fig. 6A). On the other hand, they may additionally suggest that ROS are consumed predominantly in the mitochondrial environment where they are generated. Thus local depletion of mitochondrial GSH may promote damage to the mitochondria and accelerate events leading to cell death once a critical level of damage has been surpassed. Consistent with the possibility that intracellular ROS may induce MPT resulting in mitochondrial dysfunction, ROS production prior to onset of MPT and mitochondrial depolarization have been reported in hepatocytes and hepatoma cells [52]. Furthermore, oxidants have been shown to induce MPT in isolated mitochondria [53,54] and in cells [55,56]. While we cannot exclude a possible contribution to cell demise by ROS-induced local mitochondrial damage, the observation that antioxidants did not prevent ceramide-induced MPT (Fig. 6C), but did protect against death, suggests that ROS target a cellular site other than mitochondria.

Alternative modes of cell death have been linked previously to ceramides [12,25–27]. For instance, synthetic ceramides induce a caspase-independent, necrosis-like morphology in neuro-

blastoma cells [57]. Also, ceramides kill normal lymphocytes and cell lines in the absence of caspase activation, triggering a nonapoptotic morphology in dying cells [25]. In addition, ceramide-induced cell death in leukemia cell lines was accompanied by minimal activation of caspase-3, and was not inhibited by zVAD-fmk. We previously confirmed a number of these observations in B and T lymphoma cells [12]. Mochizuki et al. [58] reported that ceramide induced cell death in human glioma cells with a necrosis-like phenotype that was efficiently inhibited by the activation of the AKT/protein kinase B pathway. Activation of JNK and p38 and increases in intracellular calcium have been associated with ceramide-induced cell death in various cell types [59–61]. All these mechanisms can potentially be activated in response to ROS formation. In order to define the extent to which activation of any one of these pathways in response to cell-permeable ceramide contributes to cell death observed here, more experiments are needed.

Ceramide has been suggested to increase cytoplasmic calcium concentrations in different types of cells. Indeed, following ceramide exposure, we observed increments in cell calcium in A20 cells using Fluo-3/AM (data not shown). In addition to ATP-dependent calcium influx, ceramide increases the $[Ca^{2+}]i$ from a thapsigargin-sensitive calcium pool and the subsequent activation of a capacitative calcium entry in human Jurkat T cells [63]. In this particular study, increased cytoplasmic calcium concentrations were linked to liberation of calcium from intracellular stores and activation of a store-operated calcium channel. On the other hand, activation of calpains, due to increased intracellular calcium concentrations, has been associated with necrotic cell death [64]. Thus, two different calpain inhibitors (10 μM ALLN, 100 μM E64D; see [65]) were evaluated in ceramide-induced necrotic cell death. Consistent with the notion that calpains were not involved in execution of necrosis, these inhibitors also had no effect (data not shown).

Nonapoptotic forms of cell death have been observed as a consequence of both blocking canonical apoptotic death and/or modulating survival signaling pathways. In particular, ceramide toxicity has been shown to lead to caspase-independent cell death accompanied by features characteristic of autophagy (see discussion in [10]). In order to evaluate whether ceramide-induced nonapoptotic cell death occurred as a consequence of induction of autophagy, the cell death in response to ceramide was evaluated in the presence of compounds (5 mM 3-methyladenine, 10 μM LY294002, or 5 nM Wortmannin) that reportedly block autophagy [66,67]. None of these inhibitors enhanced viability or modulated ceramide-induced necrotic cell death, suggesting that autophagy was not required (data not shown).

A recent report demonstrated that ceramide-induced cell death was accompanied by ATP reduction, but not by loss of mitochondrial membrane potential [27]. In contrast to this report, we suggest that C6-induced necrosis occurs as a consequence of MPT disruption of mitochondrial function and ROS production. An intriguing alternative we considered was that ROS-induced damage, possibly of DNA, might activate PARP and thereby deplete cells of ATP (see [21,22]). However, the precipitous ATP decline observed after exposure of A20 (Fig. 6D, white bars) and Jurkat (Fig. 7E, white bars) cells to C6 for 4 h was only partially blocked by the PARP inhibitor 3-ABA, without statistically significant differences. As expected, in a control experiment using Jurkat T cells, hydrogen peroxide induced both ATP depletion and necrosis that were blocked in the presence of 3-ABA (Figs. 8A and 8B), while Tiron was more effective in this respect (see Figs. 6D and 7E; gray bars). Interestingly, however, despite blocking PARP, cellular NADPH levels declined in a manner similar to that observed for ATP. Since NADPH is also employed to regenerate GSH from GSSG in the cytosol, a plausible explanation for our results is that regeneration of GSH following ceramide-induced ROS formation depleted cells of NADPH and, as a consequence, also ATP. Thus, our results, obtained in two different lymphoid cell lines, favor the interpretation that ROS of mitochondrial origin promote necrotic cell death, via ATP depletion that is likely to be linked in part to NADPH consumption as a consequence of GSH depletion.

Conclusions

In summary, we identified mitochondria as prime targets of cell-permeable ceramides, which promote mitochondrial dysfunction, ROS formation, and necrotic cell death. To what extent ceramide induces apoptotic or nonapoptotic cell death (or both) is determined by complex factors, including the cell type and the environment surrounding the cells. Our results indicate that ATP depletion following C6-induced mitochondrial ROS production is a major driving force for C6-induced necrosis in lymphoid cells. Thus, while ceramide formation has frequently been associated with apoptosis, our results suggest that regulated ceramide production at or near the mitochondria may represent a physiologically relevant mechanism to promote execution of alternative forms of cell death, such as necrosis.

Acknowledgments

The work presented here was supported by Wellcome Trust 064911/Z/01/z and ICGEB CRP/CH102-01(to A.F.G. Quest), FONDAP 15010006 (to A.F.G. Quest, S. Lavandero, and A. Stutzin), CONICYT Post-Doctoral Fellowship 3070045 (to M. Henriquez), and CONICYT Ph.D. Student Fellowships (to V. Torres and F. Moraga). Parts of the results shown here have been presented previously in preliminary form as an abstract/poster (International Symposium on Mechanism of Cell Death: Molecular Insights and Therapeutic Perspectives, Reñaca (Chile, April 2005).

References

[1] Hannun, Y. A.; Obeid, L. M. The ceramide-centric universe of lipid-mediated cell regulation: stress encounters of the lipid kind. *J. Biol. Chem.* **277:**25847–25850; 2002.

[2] Venkataraman, K.; Futerman, A. H. Ceramide as a second messenger: sticky solutions to sticky problems. *Trends Cell Biol.* **10:**408–412; 2000.

[3] Garcia-Ruiz, C.; Colell, A.; Mari, M.; Morales, A.; Fernandez-Checa, J. C. Direct efect of ceramide on the mitochondrial electron transport chain leads to generation of reactive oxygen species. Role of mitochondrial glutathione. *J. Biol. Chem.* **272:**11369–11377; 1997.

[4] Gudz, T. I.; Tserng, K. Y.; Hoppel, C. L. Direct inhibition of mitochondrial respiratory chain complex III by cell-permeable ceramide. *J. Biol. Chem.* **272:**24154–24158; 1997.

[5] Quillet-Mary, A.; Jafrezou, J. P.; Mansat, V.; Bordier, C.; Naval, J.; Laurent, G. Implication of mitochondrial hydrogen peroxide generation in ceramide-induced apoptosis. *J. Biol. Chem.* **272:**21388–21395; 1997.

[6] Raha, S.; Robinson, B. H. Mitochondria, oxygen free radicals, and apoptosis. *Am. J. Med. Genet.* **106:**62–70; 2001.

[7] Griendling, K. K. ATVB in focus: redox mechanisms in blood vessels. *Arterioscler. Thromb. Vasc. Biol.* **25:**272–273; 2005.

[8] Bai, J.; Cederbaum, A. I. Mitochondrial catalase and oxidative injury. *Biol. Signals Recept.* **10:**189–199; 2001.

[9] Han, K. S.; Kang, H. J.; Kim, E. Y.; Yoon, W. J.; Sohn, S.; Kwon, H. J.; Gwag, B. J. 1,2- Bis(2-aminophenoxy)ethane-N,N,N0,N0-tetraacetic acid induces caspase-mediated apoptosis and reactive oxygen species-mediated necrosis in cultured cortical neurons. *J. Neurochem.* **78:**230–239; 2001.

[10] Hetz, C. A.; Torres, V.; Quest, A. F. Beyond apoptosis: nonapoptotic cell death in physiology and disease. *Biochem. Cell. Biol.* **83:**579–588; 2005.

[11] Golstein, P.; Kroemer, G. Cell death by necrosis: towards a molecular definition. *Trends Biochem. Sci.* **32:**37–43; 2007.

[12] Hetz, C. A.; Hunn, M.; Rojas, P.; Torres, V.; Leyton, L.; Quest, A. F. Caspase-dependent initiation of apoptosis and necrosis by the Fas receptor in lymphoid cells: onset of necrosis is associated with delayed ceramide increase. *J. Cell Sci.* **115:**4671–4683; 2002.

[13] Eisner, V.; Criollo, A.; Quiroga, C.; Olea-Azar, C.; Santibanez, J. F.; Troncoso, R.; Chiong, M.; Diaz-Araya, G.; Foncea, R.; Lavandero, S. Hyperosmotic stress-dependent NF-kappaB activation is regulated by reactive oxygen species and IGF-1 in cultured cardiomyocytes. *FEBS Lett.* **580:**4495–4500; 2006.

[14] Anderson, M. E.; Meister, A. Dynamic state of glutathione in blood plasma. *J. Biol. Chem.* **255:**9530–9533; 1980.

[15] Emaus, R. K.; Grunwald, R.; Lemaster, J. J. Rhodamine 123 as a probe of transmembrane potential in isolated rat-liver mitochondria: spectral and metabolic properties. *Biochim. Biophys. Acta* **850:**436–448; 1986.

[16] Lam, E. W.; Zwacka, R.; Seftor, E. A.; Nieva, D. R.; Davidson, B. L.; Engelhardt, J. F.; Hendrix, M. J.; Oberley, L. W. Effects of antioxidant enzyme overexpression on the invasive phenotype of hamster cheek pouch carcinoma cells. *Free Radic. Biol. Med.* **27:**572–579; 1999.

[17] Siskind, L. J.; Kolesnick, R. N.; Colombini, M. Ceramide forms channels in mitochondrial outer membranes at physiologically relevant concentrations. *Mitochondrion* **6:**118–125; 2006.

[18] Siskind, L. J.; Kolesnick, R. N.; Colombini, M. Ceramide channels increase the permeability of the mitochondrial outer membrane to small proteins. *J. Biol. Chem.* **277:**26796–26803; 2002.

[19] Di Paola, M.; Cocco, T.; Lorusso, M. Ceramide interaction with the respiratory chain of heart mitochondria. *Biochemistry* **39:**6660–6668; 2000.

[20] Birbes, H.; El Bawab, S.; Hannun, Y. A.; Obeid, L. M. Selective hydrolysis of a mitochondrial pool of sphingomyelin induces apoptosis. *FASEB J.* **15:**2669–2679; 2001.

[21] Dawson, V. L.; Dawson, T. M. Deadly conversations: nuclear-mitochondrial cross-talk. *J. Bioenerg. Biomembranes* **36:**287–294; 2004.

[22] van Wijk, S. J.; Hageman, G. J. Poly(ADP-ribose) polymerase-1 mediated caspase-independent cell death after ischemia/reperfusion. *Free Radic. Biol. Med.* **39:**81–90; 2005.

[23] Kolesnick, R. N.; Kronke, M. Regulation of ceramide production and apoptosis. *Annu. Rev. Physiol.* **60:**643–665; 1998.

[24] Pettus, B. J.; Chalfant, C. E.; Hannun, Y. A. Ceramide in apoptosis: an overview and current perspectives. *Biochim. Biophys. Acta* **1585:**114–125; 2002.

[25] Mengubas, K.; Fahey, A. A.; Lewin, J.; Mehta, A. B.; Hoffbrand, A. V.; Wickremasinghe, R. G. Killing of T lymphocytes by synthetic ceramide is by a nonapoptotic mechanism and is abrogated following mitogenic activation. *Exp. Cell Res.* **249:**116–122; 1999.

[26] Thon, L.; Mohlig, H.; Mathieu, S.; Lange, A.; Bulanova, E.; Winoto-Morbach, S.; Schutze, S.; Bulfone-Paus, S.; Adam, D. Ceramide mediates caspase-independent programmed cell death. *FASEB J.* **19:**1945–1956; 2005.

[27] Kim, W. H.; Choi, C. H.; Kang, S. K.; Kwon, C. H.; Kim, Y. K. Ceramide induces non-apoptotic cell death in human glioma cells. *Neurochem. Res.* **30:**969–979; 2005.

[28] Granot, T.; Milhas, D.; Carpentier, S.; Dagan, A.; Segui, B.; Gatt, S.; Levade, T. Caspase-dependent and -independent cell death of Jurkat human leukemia cells induced by novel synthetic ceramide analogs. *Leukemia* **20:**392–399; 2006.

[29] Bollinger, C. R.; Teichgraber, V.; Gulbins, E. Ceramide-enriched membrane domains. *Biochim. Biophys. Acta* **1746:**284–294; 2005.

[30] Anishkin, A.; Sukharev, S.; Colombini, M. Searching for the molecular arrangement of transmembrane ceramide channels. *Biophys. J.* **90:** 2414–2426; 2006.

[31] Ueda, S.; Masutani, H.; Nakamura, H.; Tanaka, T.; Ueno, M.; Yodoi, J. Redox control of cell death. *Antioxid. Redox Signal.* **4:**405–414; 2002.

[32] Chandra, J.; Samali, A.; Orrenius, S. Triggering and modulation of apoptosis by oxidative stress. *Free Radic. Biol. Med.* **29:**323–333; 2000.

[33] Carmody, R. J.; Cotter, T. G. Signalling apoptosis: a radical approach. *Redox Rep.* **6:**77–90; 2001.

[34] Troyano, A.; Sancho, P.; Fernandez, C.; de Blas, E.; Bernardi, P.; Aller, P. The selection between apoptosis and necrosis is differentially regulated in hydrogen peroxide-treated and glutathione-depleted human promonocytic cells. *Cell Death Differ.* **10:**889–898; 2003.

[35] Ventura, J. J.; Cogswell, P.; Flavell, R. A.; Baldwin, A. S.; Davis Jr., R. J. JNK potentiates TNF-stimulated necrosis by increasing the production of cytotoxic reactive oxygen species. *Genes Dev.* **18:**2905–2915; 2004.

[36] Sakon, S.; Xue, X.; Takekawa, M.; Sasazuki, T.; Okazaki, T.; Kojima, Y.; Piao, J. H.; Yagita, H.; Okumura, K.; Doi, T.; Nakano, H. NF-kappaB inhibits TNF-induced accumulation of ROS that mediate prolonged MAPK activation and necrotic cell death. *EMBO J.* **22:**3898–3909; 2003.

[37] Ankarcrona, M.; Dypbukt, J. M.; Bonfoco, E.; Zhivotovsky, B.; Orrenius, S.; Lipton, S. A.; Nicotera, P. Glutamate-induced neuronal death: a succession of necrosis or apoptosis depending on mitochondrial function. *Neuron* **15:**961–973; 1995.

[38] Dypbukt, J. M.; Ankarcrona, M.; Burkitt, M.; Sjoholm, A.; Strom, K.; Orrenius, S.; Nicotera, P. Different prooxidant levels stimulate growth, trigger apoptosis, or produce necrosis of insulin-secreting RINm5F cells. The role of intracellular polyamines. *J. Biol. Chem.* **269:**30553–30560; 1994.

[39] Vercammen, D.; Brouckaert, G.; Denecker, G.; Van de Craen, M.; Declercq, W.; Fiers, W.; Vandenabeele, P. Dual signaling of the Fas receptor: initiation of both apoptotic and necrotic cell death pathways. *J. Exp. Med.* **188:**919–930; 1998.

[40] Davies, K. J. The broad spectrum of responses to oxidants in proliferating cells: a new paradigm for oxidative stress. *IUBMB Life* **48:**41–47; 1999.

[41] Simon, F.; Varela, D.; Eguiguren, A. L.; Diaz, L. F.; Sala, F.; Stutzin, A. Hydroxyl radical activation of a Ca(2+)-sensitive nonselective cation channel involved in epithelial cell necrosis. *Am. J. Physiol., Cell Physiol.* **287:**C963–C970; 2004.

[42] Birbes, H.; Bawab, S. E.; Obeid, L. M.; Hannun, Y. A. Mitochondria and ceramide: intertwined roles in regulation of apoptosis. *Adv. Enzyme Regul.* **42:**113–129; 2002.

[43] Shimeno, H.; Soeda, S.; Sakamoto, M.; Kouchi, T.; Kowakame, T.; Kihara, T. Partial purification and characterization of sphingosine *N*-acyltransferase (ceramide synthase) from bovine liver mitochondrion-rich fraction. *Lipids* **33:**601–605; 1998.

[44] El Bawab, S.; Roddy, P.; Qian, T.; Bielawska, A.; Lemasters, J. J.; Hannun, Y. A. Molecular cloning and characterization of a human mitochondrial ceramidase. *J. Biol. Chem.* **275:**21508–21513; 2000.

[45] De Maria, R.; Lenti, L.; Malisan, F.; d'Agostino, F.; Tomassini, B.; Zeuner, A.; Rippo, M. R.; Testi, R. Requirement for GD3 ganglioside in CD95- and ceramide-induced apoptosis. *Science* **277:**1652–1655; 1997.

[46] Birbes, H.; Luberto, C.; Hsu, Y. T.; El Bawab, S.; Hannun, Y. A.; Obeid, L. M. A mitochondrial pool of sphingomyelin is involved in TNFalpha-induced Bax translocation to mitochondria. *Biochem. J.* **386:**445–451; 2005.

[47] Sultan, I.; Senkal, C. E.; Ponnusamy, S.; Bielawski, J.; Szulc, Z.; Bielawska, A.; Hannun, Y. A.; Ogretmen, B. Regulation of the sphingosine-recycling

pathway for ceramide generation by oxidative stress, and its role in controlling c-Myc/Max function. *Biochem. J.* **393:**513–521; 2006.

[48] Guimaraes, A. C.; Linden, R. Programmed cell death. Apoptosis and alternative death styles. *Eur. J. Biochem.* **271:**1638–1650; 2004.

[49] Lemasters, J. J.; Nieminen, A. L.; Qian, T.; Trost, L. C.; Elmore, S. P.; Nishimura, Y.; Crowe, R. A.; Cascio, W. E.; Bradham, C. A.; Brenner, D. A.; Herman, B. The mitochondrial permeability transition in cell death: a common mechanism in necrosis, apoptosis and autophagy. *Biochim. Biophys. Acta* **1366:**177–196; 1998.

[50] Armstrong, J. S. The role of the mitochondrial permeability transition in cell death. *Mitochondrion* **6:**225–234; 2006.

[51] Leist, M.; Single, B.; Castoldi, A. F.; Kuhnle, S.; Nicotera, P. Intracellular adenosine triphosphate (ATP) concentration: a switch in the decision between apoptosis and necrosis. *J. Exp. Med.* **185:**1481–1486; 1997.

[52] Nieminen, A. L.; Byrne, A. M.; Herman, B.; Lemasters, J. J. Mitochondrial permeability transition in hepatocytes induced by t-BuOOH:- NAD(P)H and reactive oxygen species. *Am. J. Physiol.* **272:**C1286–C1294; 1997.

[53] Valle, V. G.; Fagian, M. M.; Parentoni, L. S.; Meinicke, A. R.; Vercesi, A. E. The participation of reactive oxygen species and protein thiols in the mechanism of mitochondrial inner membrane permeabilization by calcium plus prooxidants. *Arch. Biochem. Biophys.* **307:**1–7; 1993.

[54] Colell, A.; Garcia-Ruiz, C.; Mari, M.; Fernandez-Checa, J. C. Mitochondrial permeability transition induced by reactive oxygen species is independent of cholesterol-regulated membrane fluidity. *FEBS Lett.* **560:**63–68; 2004.

[55] Vieira, H. L.; Belzacq, A. S.; Haouzi, D.; Bernassola, F.; Cohen, I.; Jacotot, E.; Ferri, K. F.; El Hamel, C.; Bartle, L. M.; Melino, G.; Brenner, C.; Goldmacher, V.; Kroemer, G. The adenine nucleotide translocator: a target of nitric oxide, peroxynitrite, and 4-hydroxynonenal. *Oncogene* **20:**4305–4316; 2001.

[56] Kanno, T.; Sato, E. E.; Muranaka, S.; Fujita, H.; Fujiwara, T.; Utsumi, T.; Inoue, M.; Utsumi, K. Oxidative stress underlies the mechanism for Ca(2+)-induced permeability transition of mitochondria. *Free Radic. Res.* **38:** 27–35; 2004.

[57] Ramos, B.; Lahti, J. M.; Claro, E.; Jackowski, S. Prevalence of necrosis in C2-ceramide-induced cytotoxicity in NB16 neuroblastoma cells. *Mol. Pharmacol.* **64:**502–511; 2003.

[58] Mochizuki, T.; Asai, A.; Saito, N.; Tanaka, S.; Katagiri, H.; Asano, T.; Nakane, M.; Tamura, A.; Kuchino, Y.; Kitanaka, Ch.; Kirino, T. Akt protein kinase inhibits non-apoptotic programmed cell death induced by ceramide. *J. Biol. Chem.* **277:**2790–2797; 2002.

[59] Waring, P. Redox active calcium ion channels and cell death. *Arch. Biochem. Biophys.* **434:**33–42; 2005.

[60] Westwick, J. K.; Bielawska, A. E.; Dbaibo, G.; Hannun, Y. A.; Brenner, D. A. Ceramide activates the stress-activated protein kinases. *J. Biol. Chem.* **270:**22689–22692; 1995.

[61] Willaime, S.; Vanhoutte, P.; Caboche, J.; Lemaigre-Dubreuil, Y.; Mariani, J.; Brugg, B. Ceramide-induced apoptosis in cortical neurons is mediated by an increase in p38 phosphorylation and not by the decrease in ERK phosphorylation. *Eur. J. Neurosci.* **13:**2037–2046; 2001.

[62] Nakamura, J.; Asakura, S.; Hester, S. D.; de Murcia, G.; Caldecott, K. W.; Swenberg, J. A. Quantitation of intracellular NAD(P)H can monitor an imbalance of DNA single strand break repair in base excision repair deficient cells in real time. *Nucleic Acids Res.* **31:**e104; 2003.

[63] Colina, C.; Flores, A.; Rojas, H.; Acosta, A.; Castillo, C.; Garrido, M. R.; Israel, A.; Dipolo, R.; Benaim, G. Ceramide increase cytoplasmic Ca^{2+} concentration in Jurkat T cells by liberation of calcium from intracellular stores and activation of a store-operated calcium channel. *Arch. Biochem. Biophys.* **436:**333–345; 2005.

[64] Harwood, S. M.; Allen, D. A.; Raftery, M. J.; Yaqoob, M. M. High glucose initiates calpain-induced necrosis before apoptosis in LLC-PK1 cells. *Kidney Int.* **71:**655–663; 2007.

[65] Felley-Bosco, E.; Bender, F. C.; Courjault-Gautier, F.; Bron, C.; Quest, A. F. Caveolin-1 down-regulates inducible nitric oxide synthase via the proteasome pathway in human colon carcinoma cells. *Proc. Natl. Acad. Sci. U. S. A.* **97:**14334–14339; 2000.

[66] Blommaart, E. F.; Krause, U.; Schellens, J. P.; Vreeling-Sindelarova, H.; Meijer, A. J. The phosphatidylinositol 3-kinase inhibitors wortmannin and LY294002 inhibit autophagy in isolated rat hepatocytes. *Eur. J. Biochem.* **243:**240–246; 1997.

[67] Plo, I.; Bettaieb, A.; Payrastre, B.; Mansat-De, M. V.; Bordier, C.; Rousse, A.; Kowalski-Chauvel, A.; Laurent, G.; Lautier, D. The phosphoinositide 3-kinase/Akt pathway is activated by daunorubicin in human acute myeloid leukemia cell lines. *FEBS Lett.* **452:**150–154; 1999.